Teknomekanik, Vol. 9, No. 2, 2026, pp. 137-161
e-ISSN: 2621-8720 p-ISSN: 2621-9980

Comparative study on the corrosion behavior of TiCN-coated austenitic and ferritic stainless steels in geothermal environments

Agus Solehudin[1*], Haipan Salam[1], Enda Permana[2], Atiek Rostika Noviyanti[3], Akrajas Ali Umar[4] and Risti Ragadhita[1]

[1] Study Program of Chemical Engineering, Faculty of Engineering and Industrial Education, Universitas Pendidikan Indonesia, **Indonesia**
[2] Study Program of Mechanical Engineering Education, Faculty of Engineering and Industrial Education, Universitas Pendidikan Indonesia, **Indonesia**
[3] Study Program of Chemistry, Faculty of Mathematics and Natural Sciences, Universitas Padjajaran, **Indonesia**
[4] Institute of Microengineering and Nanoelectronics, Universiti Kebangsaan Malaysia, **Malaysia**

*Corresponding Author: asolehudin@upi.edu
Received: 20 August 2025; *Revised:* 23 April 2026; *Accepted:* 30 April 2026

Cite this https://doi.org/10.24036/teknomekanik.v9i2.44172

Abstract: Corrosion in stainless steel (SS) remains a critical limitation for its application, particularly in harsh environments such as geothermal systems. This study aims to evaluate the corrosion resistance of two SS substrates, namely SS 11-0 (ferritic) and SS 18-8 (austenitic), used as drill bit materials, both before and after the application of a TiCN protective coating. The coating was deposited by Physical Vapor Deposition (PVD) for 15, 25, and 35 minutes at 250°C. Corrosion resistance was assessed using a salt spray test with a 5% NaCl solution (pH 6–7) for 100 hours to simulate a neutral corrosive environment. Surface morphology and elemental composition were characterized using Field Emission Scanning Electron Microscopy–Energy Dispersive X-ray Spectroscopy (FESEM–EDS), while coating thickness and hardness were evaluated using Fischerscope® X-RAY XAN and Vickers microhardness testing, respectively. Corrosion performance was quantitatively analyzed using mass-loss-based corrosion rate calculations and polarization resistance measurements with a potentiostat instrument, providing insights into the electrochemical behavior of the coating–substrate system. The results demonstrate that increasing deposition time enhances coating thickness and overall coating quality. FESEM–EDS analysis confirms the successful formation of the TiCN layer and reveals changes in surface morphology and elemental composition after coating and corrosion exposure. Among the tested substrates, SS 18-8 consistently exhibits superior hardness, surface uniformity, and corrosion resistance compared to SS 11-0. Based on the weight loss method, the corrosion rates of uncoated and TiCN-coated SS 18-8 are 0.2600 mm/year and 0.1625 mm/year, respectively, both lower than those observed for SS 11-0. This enhanced performance is attributed to the synergistic effect between the TiCN coating and the Cr- and Ni-rich chemical composition of SS 18-8, which facilitates the formation of a stable and protective passive layer. These findings highlight the strong potential of TiCN-coated SS 18-8 for applications in geothermal environments under neutral corrosive conditions.

Keywords: corrosion resistance; geothermal condition; PVD; polarization resistance; stainless steel; weight loss

1. Introduction

Currently, as global demand for sustainable energy increases, countries are increasingly seeking to harness and utilize geothermal resources [1], [2]. To harness geothermal resources, hot fluids are extracted from beneath the Earth's surface. Geothermal energy originates from the Earth's internal heat. This heat is generated by the continuous decay of radioactive materials, combined with

convective movements in the Earth's mantle. These processes then trigger the formation of hotspots and volcanic activity, which ultimately heat the fluids within the Earth's crust. These hot fluids can be channeled to the surface to be utilized as a heat source or for power generation [3]. One current challenge in utilizing geothermal resources for power generation is managing corrosive geothermal fluids. Various studies have shown that geological conditions and the operational history of geothermal wells play a role in creating variations in operating temperatures and the chemical composition of the water within them [4], [5].

Based on various previous studies, the chemical composition of geothermal water is highly complex. According to Bai et al. [6], geothermal fluids contain a variety of dissolved substances such as oxygen, chloride ions (Cl^-), sulfate (SO_4^{2-}), hydrogen ions (H^+), as well as dissolved gases such as H_2S, CO_2, and NH_3, most of which are corrosive to materials. Additionally, the presence of ions such as Ca^{2+}, Mg^{2+}, CO_3^{2-}, and SO_4^{2-} can also trigger scaling on equipment surfaces. Furthermore, Rowe et al. [7] explain that geothermal fluids generally exhibit acidic properties influenced by the presence of compounds such as hydrogen chloride (Cl-type) and sulfuric acid (SO_4-type), both of which are primary causes of "ultra-acidic brines," significantly increasing the risk of corrosion in geothermal systems. Therefore, materials with high wear resistance are essential during geothermal well drilling, as downhole equipment (such as drill pipes, drill collars, stabilizers, and drill bits) is continuously exposed to geothermal environmental conditions.

Simultaneous exposure to these conditions can accelerate the rate of corrosion and gradual loss of function [8], [9]. Various forms of corrosion can have a significant impact on the efficiency, reliability, and lifespan of geothermal systems, where these forms of corrosion include: (i) uniform corrosion which occurs when the entire surface of the material is uniformly thinned due to exposure to acidic or alkaline fluids; (ii) pitting corrosion causes localized damage in the form of small holes on the metal surface which is mainly triggered by the presence of chloride ion species; (iii) galvanic corrosion which occurs when two different types of metal come into contact with one metal experiencing faster degradation; (iv) corrosion cracking caused by a combination of tensile stress and exposure to a corrosive environment; (v) corrosion erosion due to a combination of mechanical wear and chemical attack that rapidly destroys the material; (vi) hydrogen damage where the metal is exposed to hydrogen sulfide (H_2S) which causes brittle fracture; and (vii) carbon dioxide corrosion which occurs when dissolved CO_2 reacts with water to form carbonic acid, which degrades carbon steel [10]. Given the extreme conditions in the geothermal environment, maintaining infrastructure is crucial as limitations or failures can significantly disrupt system performance and reliability.

Several studies indeed show that stainless steel (SS) is one of the general materials that is superior for applications in geothermal environments (such as for pipe infrastructure, turbine components, and heat exchanger tubes) because of its superior resistance to uniform corrosion and pitting corrosion [5], [11]. Due to their superior properties, SS materials are commonly used in applications that require high corrosion resistance and mechanical resistance. However, selecting the right SS material is crucial, as geothermal conditions can vary widely from one location to another. Corrosion resistance in SS material is very dependent on the presence of the chromium elements in the form of a thin and stable layer of trivalent chromium oxide (Cr_2O_3) where the minimum amount to form a passive layer on the metal surface to prevent corrosion is around 10.5%, as well as the presence of other elements such as nickel [12], [13]. Corrosion inhibition occurs by suppressing the release of metal ions, thereby maintaining the surface in a passive state [12]. However, this resistance is not absolute, especially when SS is used in environments continuously exposed to aggressive conditions (such as marine applications or industrial systems with exposure to strong electrolytes) [5], in which case SS is susceptible to various forms of corrosion.

Environmental conditions can be optimized to maintain the performance, durability, sustainability, and service life of stainless steel through careful selection, especially regarding the presence and concentration of corrosive ions in the environment [14]. When the concentration of corrosive ions reaches a threshold, the oxide layer on stainless steel may be disrupted. Various strategies have been implemented to preserve the corrosion resistance, mechanical strength, and overall durability of SS materials. These approaches include the application of protective coatings, the use of corrosion inhibitors, and careful management of ion levels in the environment [15]. Recent advances in surface engineering have highlighted the growing interest in hard ceramic coatings deposited via physical vapor deposition (PVD) to enhance the performance of stainless-steel substrates in aggressive environments.

Titanium carbonitride (TiCN) coatings have emerged as a promising option for stainless steel 304 (SS 304) due to the synergistic effects of titanium, carbon, and nitrogen, along with their inherent corrosion resistance and cost-effectiveness. TiCN exhibits superior hardness, lower friction, and improved corrosion resistance, which are attributed to the role of titanium in enhancing adhesion and corrosion resistance, carbon in improving electrical properties, and nitrogen in stabilizing the structure [16], [17]. In addition, TiCN coatings are widely recognized for their low internal stress, excellent tribological performance, and non-toxic characteristics, making them suitable as protective layers. The performance of TiCN is also strongly influenced by its composition, particularly carbon content. At optimal levels, the formation of α-CNx phases can enhance electrochemical stability, whereas excessive carbon may lead to graphitic α-C formation that degrades corrosion resistance in aggressive environments [18]. From a processing perspective, TiCN coatings deposited using chemical vapour deposition (CVD) have been shown to produce homogeneous and dense films with well-defined interfaces, which can act as effective barriers against oxygen and aggressive ions [19]. Similarly, PVD-deposited TiCN coatings have demonstrated improved mechanical properties such as hardness and wear resistance due to their uniform distribution on the substrate [20]. Previous studies have demonstrated that TiCN coatings exhibit superior performance in protecting substrates from corrosive species, both as single coatings and in multicomponent systems. The deposition of TiCN is commonly performed using PVD, which provides excellent control over coating thickness, composition, and microstructure, resulting in dense, well-adhered films. This method has been widely recognized as an effective approach for enhancing surface performance under extreme environmental conditions, including high temperatures and highly corrosive media.

Although numerous studies have investigated the effects of coating composition and deposition parameters on microstructure and mechanical properties, research specifically addressing corrosion performance remains relatively limited. Furthermore, the influence of substrate type on the effectiveness of PVD-deposited TiCN coatings has not been systematically examined. In particular, a direct comparative study of TiCN coatings applied on SS 11-0 ferritic and SS 18-8 austenitic stainless steels, which differ significantly in chromium and nickel content, is still lacking, despite the critical role these elements play in determining coating adhesion, stability, and corrosion resistance. To address this gap, the present study provides a systematic comparative investigation of TiCN coatings on both substrate types, with a primary focus on their corrosion behavior under simulated corrosive conditions. In addition to conventional salt spray testing, electrochemical characterization using potentiostatic measurements is incorporated to provide quantitative insight into corrosion kinetics and interfacial behavior. Electrochemical techniques enable the evaluation of parameters, such as polarization resistance, that are essential for a more comprehensive assessment of coating performance beyond visual or mass loss observations [21]. The findings of this study are expected to provide fundamental insights into the role of substrate composition and coating–substrate interactions in governing corrosion performance, as well as practical guidance for optimizing TiCN coating systems to enhance durability and reliability in aggressive environments such as geothermal applications.

2. Material and methods

This study employed a systematic experimental approach integrating coating deposition, material characterization, and corrosion evaluation to assess the performance of TiCN coatings on stainless steel substrates. Two types of stainless steel, SS 18-8 (austenitic) and SS 11-0 (ferritic), were selected to examine the influence of alloy composition on coating behavior. TiCN coatings were deposited using the Physical Vapor Deposition (PVD) method under controlled vacuum conditions to ensure the formation of uniform, dense, and well-adhered films with varying thicknesses. Surface morphology and elemental composition were characterized using Field Emission Scanning Electron Microscopy–Energy Dispersive X-ray Spectroscopy (FESEM–EDS), while coating thickness and hardness were measured using Fischerscope® X-RAY XAN and Vickers microhardness testing, respectively. Corrosion performance was evaluated through a 100-hour neutral salt spray test in accordance with ASTM B117, followed by quantitative analysis using mass-loss-based corrosion rate calculations per ASTM G31, and electrochemical assessment via polarization resistance measurements.

2.1 Stainless steel substrate preparation

The substrate used in this research was stainless steel (SS), consisting of two SS categories: SS 18-8 (austenitic) and SS 11-0 (ferritic). These two types of SS substrates have different chemical compositions, where SS 18-8 contains 18% chromium and 10% nickel. However, SS 11-0 contains only 16% chromium and little to no nickel content (see Table 1) [22]. Differences in composition lead to different property characteristics. Ferritic stainless steel has a body-centered cubic (BCC) α phase, and austenitic stainless steel has a face-centered cubic (FCC) γ phase [23]. In terms of corrosion, ferritic stainless steel generally has lower resistance to pitting and crevice corrosion compared to austenitic types, making it less durable in highly aggressive chloride environments [24]. On the other hand, austenitic stainless steel, with a face-centered cubic (FCC) structure and higher nickel (Ni) content, exhibits excellent toughness, ductility, and superior general corrosion resistance [23]. However, both types of SS have weaknesses: austenitic is susceptible to stress corrosion cracking (SCC) in high-temperature environments and is rich in chloride species, while ferritic is susceptible to localized corrosion.

The ASTM G1-03(2017) e1 standard was used as a guide for preparing SS substrate surfaces, ensuring they were clean, uniform, and free from contaminants that could affect test results. The substrate surface preparation stages follow the following steps: (i) sanding the substrate surface using sandpaper with a roughness level (grit) varying between 400 to 1200 grit to remove oxide layers, rust, dirt, and microscopic imperfections on the metal surface to increase the adhesion of the coating material; (ii) cleaning the substrate with alcohol to remove dust particles, oil, and other remaining contaminants that may adhere to the surface after the sanding process, thereby ensuring the surface is completely clean before coating; (iii) dry the substrate using natural air to avoid the formation of new oxides due to contact with moist air or re-contamination from dust in the surrounding environment.

Table 1. Detailed chemical compositions of both stainless steels [22]

SS type	C	Si	Mn	P	S	Ni	Cr
SS 11-0 (Ferritic)	0.04	0.24	0.32	0.23	0.002	0.08	16.1
SS 18-8 (Austenitic)	0.02	0.70	1.49	0.03	0.00	10.8	18.3

2.2 TiCN coating process on substrate using PVD method

The method used to coat the surfaces of austenitic and ferritic substrates is Physical Vapor Deposition (PVD), which was equipped with a thermal evaporation system in a high-vacuum chamber at 250 °C, with a pressure of around 1 x 10^{-5} Torr. The vacuum pressure was set very low to remove air particles and impurities that can cause oxidation or contamination during the coating process, thereby affecting the final quality of the coating. In the coating process, the TiCN coating material is heated to its vaporization point, where it changes to vapor. TiCN vapor moves freely in the vacuum chamber towards the SS substrate prepared in the deposition chamber. The coating material sticks to the substrate due to differences in pressure and temperature, which cause its vapor to condense on the substrate's cooler surface. This causes it to stick and form a thin, even layer on the substrate. This means that the process of attaching the coating material to the substrate occurs physically without using a chemical reaction, the layer is formed due to a phase change from vapor to solid. Next, for further analysis, thickness adjustments were made by varying TiCN deposition time to 15, 25, and 35 minutes. Maintaining a controlled substrate temperature is widely recognized as a critical factor in achieving stable coating quality. Previous studies have shown that coating characteristics, including thickness and uniformity, are influenced by multiple process parameters, such as chamber pressure [25], partial pressures of carrier and reactive gases [26], power input and source type [27], applied bias voltage [28], processing temperature [29], and the sputtering yield of the target material [30] by promoting improved atomic mobility during film growth [31]. However, it should be noted that the present study does not systematically investigate the effect of substrate temperature on coating adhesion or thickness uniformity. Instead, a temperature of 250 °C was selected as a fixed and controlled parameter to ensure consistent deposition conditions across all samples.

2.3 Physicochemical characterization test: Coating thickness analysis

The physicochemical characteristics of the substrate surface before and after the coating process were analyzed using Field Emission Scanning Electron Microscopy (FESEM-EDS; Sigma 360 Carl Zeiss). FESEM was used to observe surface morphology and topography at high resolution, thereby identifying changes in surface structure, including roughness, coating homogeneity, and the presence of defects, such as pores, cracks, or pinholes, resulting from the coating process. Meanwhile, EDS was used to analyze the elemental composition of the material surface, both qualitatively and semi-quantitatively, to confirm the presence and distribution of the coating's constituent elements on the substrate. The thickness of the TiCN layer deposited on the substrate was measured using a Fischerscope® X-Ray XAN instrument at several random points on the substrate surface to avoid bias and obtain representative and accurate data. The thickness before and after the coating process was then compared, thus the increase in thickness of the TiCN layer formed as the coating process increases over time could be determined. This information is important to correlate the effect of coating time on coating quality, especially in terms of thickness which has the potential to influence hardness characteristics.

2.4 Mechanical characteristics test: Coating hardness test

Mechanical tests (hardness) were performed on substrate specimens before and after TiCN coating to evaluate the impact of coating time on surface mechanical properties. The Vickers method with a specified test load was used to measure the hardness of the specimen at several random points on its surface to ensure the data obtained were representative and accurate. Testing before the coating process helps determine the SS material's original hardness. After coating, hardness testing determines changes in hardness caused by the formation of the TiCN layer. Variations in deposition time significantly affect the thickness of the TiCN layer. This thickness is closely related to increased surface hardness, as thicker layers generally provide better mechanical protection.

2.5 Corrosion performance test in a neutral environment through the salt spray method

The ASTM B117 standard method was used as a guide to carry out corrosion testing on SS 18-8 and SS 11-0 specimens before and after coated with TiCN via the salt spray method. This corrosion test was conducted to assess how well a coating withstands a corrosive environment. The corrosion test was carried out by spraying a salt solution with a concentration of 5% w/v, with a pH ranging from 6.5 to 7.2 continuously on the specimen in an airtight chamber where the temperature was maintained at 35 ± 2 °C with a falling mist volume of 1.0 to 2.0 mL/80 cm² per hour with a test duration of 100 hours (medium-term exposure simulation). During testing, the pH and volume of the mist deposits are periodically controlled to maintain stable test conditions. At the testing time, samples were collected from the chamber, cleaned with deionized water, and dried before analysis.

Evaluation was carried out by observing the presence of corrosion products. To evaluate the corrosion rate based on mass loss, the ASTM G31 standard method was used. The corrosion rate is calculated using Equation 1.

$$Cr = \frac{\text{kW}}{DAT} \tag{1}$$

Where Cr is corrosion rate (µm/y = micrometer of penetration per year), k is constant (8.76 x 107), W is weight loss (g), A is outer exposed surface (cm^2), T is time (hour), and D is the density of the material exposed to the corrosive environment, i.e., the substrate material for the uncoated specimen and the coating material for the coated specimen.

Electrochemical corrosion testing was also conducted using the linear polarization resistance method using a potentiostat (Gamry Instrument Reference 3000) to quantitatively evaluate the corrosion resistance. The measurements were performed using a conventional three-electrode system, consisting of the coated or uncoated specimen as the working electrode (substrate), a platinum electrode as the counter electrode, and an Ag/AgCl electrode as the reference electrode. The electrolyte used was a 3.5 wt% NaCl solution at room temperature. Prior to measurement, the specimens were immersed in the electrolyte for a stabilization period to reach a steady open circuit potential (OCP). Potentiodynamic polarization tests were carried out by sweeping the potential from −0.03 mV to +0.03 mV versus OCP at a scan rate of 0.167 mV/s. The resulting linear polarization resistance (LPR) curves were analyzed using Tafel extrapolation to determine key electrochemical parameters, including corrosion current density (I_{corr}), polarization resistance (Rp), and corrosion rate. These parameters provide insight into the corrosion kinetics and the protective performance of the TiCN coating. In polarization resistance testing, I_{corr}, Rp, and corrosion rate are interrelated in describing corrosion behavior. I_{corr} indicates the corrosion reaction rate; thus, the higher the value, the higher the corrosion rate. The corrosion rate is a quantitative measure of material degradation, which is proportional to I_{corr}. Meanwhile, Rp reflects the material's resistance to corrosion and is inversely proportional to both I_{corr} and the corrosion rate. Thus, materials with low I_{corr} and corrosion rate values and a high Rp value exhibit better corrosion resistance.

3. Results and discussion

3.1 Elemental and morphological characterization for uncoated and coated substrate

Figure 1(a–d) presents a comparative analysis of the EDS spectra, demonstrating that variations in spectral profiles correspond to differences in the chemical composition of the substrate surfaces. These compositional differences play a crucial role in determining the corrosion resistance of each

substrate. The EDS results for SS 11-0 and SS 18-8 substrates prior to coating are shown in Figure 1(a–b), while the corresponding results after TiCN coating are presented in Figure 1(c–d). The SS 11-0 substrate is characterized by a relatively low alloy content, predominantly composed of Fe (84.65%) and Cr (12.09%), with no detectable Ni. This composition renders the material more susceptible to corrosion, particularly in chloride-containing environments [12], [13]. These findings are consistent with previous studies, which report that SS 11-0 typically contains high Fe content (>80%), moderate Cr content 10–18%, and little to no Ni addition [32], [33], [34]. Moreover, the Cr content in SS 11-0 is generally limited to approximately 11–12% for cost-efficiency considerations, thereby reducing its corrosion resistance [35]. Overall, the compositional characteristics identified by EDS analysis confirm that SS 11-0 can be classified as a ferritic stainless steel with relatively lower corrosion resistance than alloy systems containing higher Cr and Ni contents [12], [13], [35].

The EDS results for the SS 18-8 substrate (Figure 1(b)) indicate a lower Fe content (65.25%), which is largely substituted by alloying elements, particularly Cr (16.95%) and Ni (7.08%). The higher chromium content promotes the formation of a stable and protective passive layer, primarily composed of Cr_2O_3, thereby enhancing corrosion resistance. In addition, nickel plays a crucial role in stabilizing the austenitic phase and improving resistance to intergranular corrosion and oxidation processes [36], [37]. A minor amount of Mn (0.13%) was also detected in the SS 18-8 substrate. Manganese functions as a deoxidizing agent during steel processing and contributes to the development of a more uniform microstructure [37], [38]. These compositional characteristics are consistent with the fundamental behavior of austenitic stainless steels, where the synergistic interaction between Cr and Ni significantly enhances both corrosion resistance and mechanical performance. High concentrations of Cr and Ni are known to facilitate the spontaneous formation of a dense, stable, and adherent passive film, thereby improving the overall durability of the material in corrosive environments [39], [40].

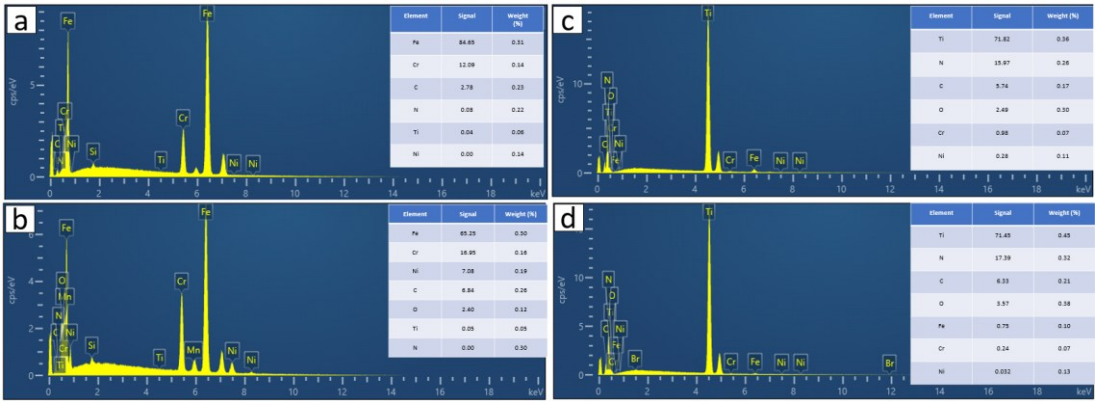

Figure 1. EDS results for (a) SS 11-0 and (b) SS 18-8 before coating as well as for (c) SS 11-0 and (d) SS 18-8 after coating with TiCN

The SS 18-8 substrate has a higher carbon content (6.84%) than the SS 11-0 substrate (2.78%). This carbon level remains within the acceptable range for austenitic stainless steels, where carbon can be accommodated in relatively higher amounts due to its greater solubility in the austenitic matrix. This characteristic helps minimize the formation of chromium carbides, thereby reducing the risk of chromium depletion at grain boundaries and maintaining corrosion resistance [41]. In contrast, ferritic stainless steels such as SS 11-0 have significantly lower carbon solubility. As a result, even small amounts of carbon can promote the formation of chromium carbides, leading to localized chromium depletion. This phenomenon weakens the passive film, creating preferential sites for localized corrosion, including pitting and intergranular corrosion. Furthermore, the relatively higher atomic mobility in ferritic structures can accelerate carbide formation, making

them more susceptible to corrosion-related degradation [12], [13]. The EDS results, which indicate higher Cr and Ni contents in the SS 18-8 substrate, further support its superior corrosion resistance compared to SS 11-0 [42], [43]. The synergistic effect of these alloying elements enhances the stability of the passive layer, thereby improving the material's overall resistance to aggressive environments.

Figures 1(c) and 1(d) present the EDS analysis results for the SS 11-0 and SS 18-8 substrates after TiCN coating, respectively. The spectra are dominated by titanium (Ti), followed by nitrogen (N), carbon (C), and oxygen (O), confirming the successful formation of the TiCN layer. Although substrate-derived elements, such as Fe, Cr, and Ni, are still detectable, their intensities are significantly reduced (below 1%), indicating that the TiCN coating effectively covers the substrate surface with high uniformity.

Apart from EDS analysis, FESEM analysis (Figure 2(a-d)) was also carried out to evaluate the success of the coating process, and to observe the surface microstructure, layer compactness, and the presence of defects or irregularities after coating. Figures 2(a) and 2 (c) show the SS 11-0 and SS 18-8 substrates before coating, respectively. Based on the FESEM analysis, both substrates exhibit a surface morphology dominated by elongated grooves. The SS 18-8 substrate shows a more well-defined and pronounced groove structure (see Figure 2(c)) compared to the SS 11-0 substrate (see Figure 2(a)). These grooves are likely associated with machining-induced features, possibly originating from defects or wear on the working surface of the fabrication tools. The presence of grooves indicates that the substrate is not protected and is very susceptible to corrosion, because the metal surface is directly exposed to environmental factors such as air, water vapor, chemical compounds, and aggressive ions such as Cl^- and SO_4^{2-}. Micro-defects such as scratches, fine cracks, or pores also serve as starting points for corrosion, as they increase the contact area and provide pathways for corrosive substances [8], [12], [44]. These observations suggest that surface morphology likely influences corrosion and wear behavior. Smoother surfaces (as observed in uncoated SS 11-0) are expected to improve wear resistance by reducing the contact area and minimizing abrasive interactions, whereas rougher surfaces (as SS 18-8 uncoating) are predicted to increase the corrosion rate by providing more active sites for electrochemical reactions [45], [46].

Figures 2(b) and 2(d) present the FESEM characterization of SS 11-0 and SS 18-8 substrates after TiCN deposition. The coated substrates exhibit a clear transformation in surface topography, with the TiCN layer forming a relatively smooth, homogeneous, and uniformly distributed coating. Surface characteristics are generally associated with improved adhesion between the coating and the substrate [47]. Nevertheless, several growth-related defects, including macroscopic pinholes and macroparticles, are still observed (see Figure 2(b and d)). Although the passive film formed by the coating possesses high resistance to ionic diffusion, the presence of these defects locally compromises its protective capability. In particular, pinholes, which are microscopic defects that partially or fully penetrate the coating layer, are typically associated with non-ideal deposition conditions, such as contamination or gas entrapment during the process [47]. The presence of pinholes as initial defects plays a critical role in initiating corrosion within the coating and substrate system. These discontinuities provide pathways for aggressive species to infiltrate the coating and reach the more electrochemically active substrate. Once penetration occurs, localized corrosion reactions are triggered beneath the pinhole sites [48]. The corrosion products formed generally occupy a larger volume than the parent metal, leading to internal stresses within the overlying coating layer. The progressive accumulation of these stresses can induce cracking and, eventually, flake detachment, as reported in Cr/a-C multilayer systems [49]. Following the breakdown of the passive layer, localized corrosion phenomena such as pitting corrosion may occur, characterized by the formation of deep and confined cavities on the steel surface. The degradation of the passive film facilitates increased anodic dissolution of Fe and Cr, further accelerating the corrosion process. Consequently, this damage evolution generates secondary diffusion pathways that enhance the

ingress of corrosive species, thereby promoting the expansion of degradation zones and accelerating the overall deterioration of the coating system [49], [50].

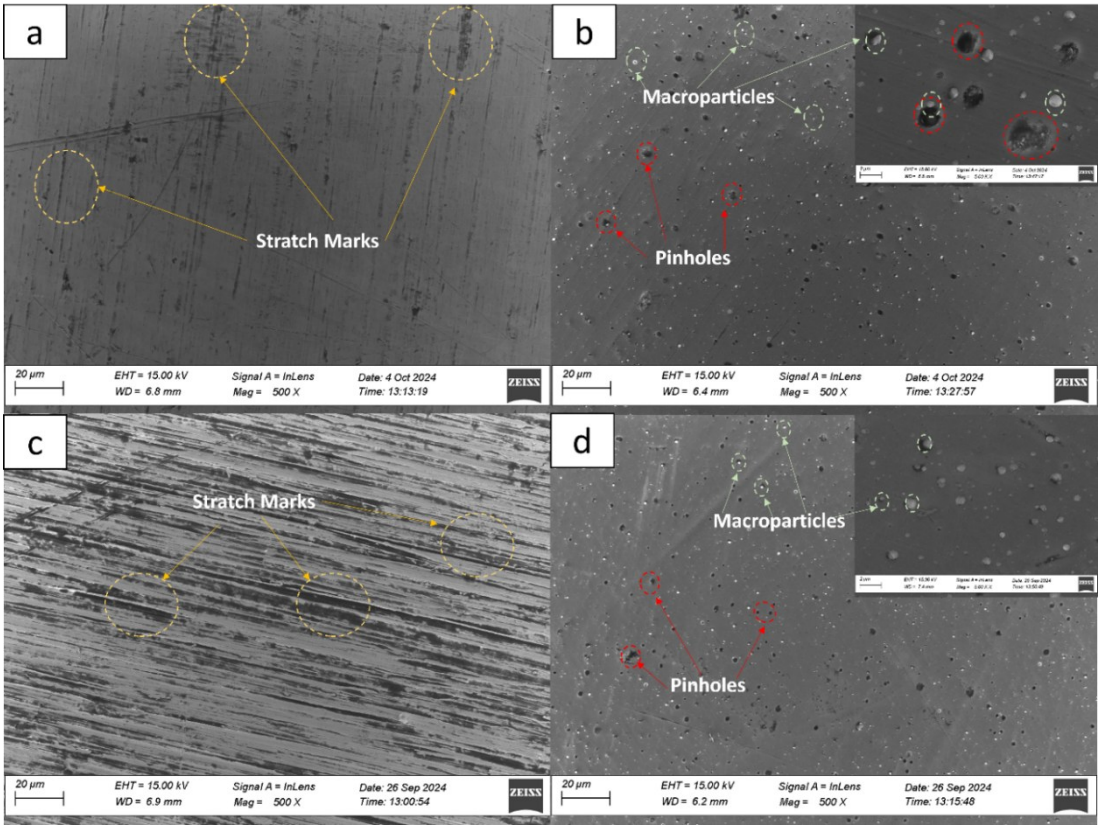

Figure 2. Surface morphology of SS 11-0 before (a) and after coating (b) and surface morphology of SS 18-8 before (c) and after (d) TiCN coating using the PVD method where the inset shows an enlargement of surface defects in the form of pinholes and macroparticles typical of the coating results

Meanwhile, macroparticles (droplets) appear as round protrusions which can cause the surface to become rough, inhomogeneous, and reduce adhesion to the substrate [51], [52]. The presence of macroparticles (droplets) formed during the deposition process also significantly contributes to a decline in coating performance. Macroparticles typically appear as round protrusions on the surface, leading to increased roughness, morphological irregularities, and thickness inhomogeneity [51], [52]. Their presence not only contaminates the substrate surface but also creates weak interfacial bonds due to limited bonding between the droplets and the substrate material. This condition directly impacts the overall reduction in coating adhesion, creating weak points that are susceptible to crack initiation and delamination [53]. Furthermore, macroparticles also play a role in the formation of secondary defects, such as pores and pinholes, due to imperfect layer growth around them, which acts as a diffusion pathway for corrosive species [53]. Defects such as pinholes and macroparticles in TiCN coatings can significantly affect long-term corrosion resistance, particularly in aggressive geothermal environments. Under high-temperature, high-pressure conditions, coupled with the presence of corrosive ions such as Cl^-, these defects facilitate the ingress of corrosive species into the coating and weaken the bond between the coating and the substrate. Additionally, the uneven surface caused by macroparticles and the presence of small gaps due to pinholes make the coating more susceptible to damage, particularly when subjected to repeated changes in temperature and chemical conditions. Over time, these conditions lead to a gradual decline in the coating's protective quality, resulting in a shorter service life and an increased risk of premature failure. Therefore, controlling these defects is crucial for maintaining optimal coating performance over the long term.

The coating formed on the SS 18-8 substrate (see Figure 2(d)) exhibits a higher degree of uniformity and surface smoothness compared to that on SS 11-0 (see Figure 2(b)). This behavior is attributed to the relatively higher initial surface roughness of SS 18-8 (as shown in Figure 2(c)), which facilitates more effective nucleation, lateral growth, and redistribution of deposited species during the PVD process, thereby improving layer spreading and surface leveling [54]. This observation is consistent with previous studies reporting that excessively smooth substrates (as shown in the SS 11-0 substrate in Figure 2(a)) may hinder coating adhesion due to limited mechanical interlocking and reduced nucleation sites [55]. According to the literature, adequate surface roughness facilitates effective coating spreading and leveling, thereby promoting stronger interfacial interactions that are essential for optimal adhesion [56]. Conversely, coatings that are uneven or discontinuous tend to exhibit weaker adhesion and are more susceptible to delamination under mechanical or environmental stress. In corrosive environments, such degradation can further accelerate electrochemical processes, including localized and galvanic corrosion [57], [58]. However, in this study, the initial roughness of the substrate (in SS 18-8 substrate as shown in Figure 2(b)) contributes positively by enhancing coating uniformity through improved deposition dynamics. Therefore, it is important to distinguish the dual role of surface roughness in coating performance. Roughness arising from growth-related defects, particularly macroparticles, exhibits fundamentally different characteristics and may be detrimental. Such defect-induced irregularities can introduce local inhomogeneities, weaken interfacial bonding, and create stress concentration sites that compromise coating integrity [51], [53]. Although this aspect is not systematically investigated in the present study, previous works [51], [53] suggest that these conditions may reduce long-term corrosion resistance, especially in aggressive environments such as geothermal applications.

The images in Figures 2(b) and 2(d) are higher-magnification views of some surface areas after coating, clearly showing the pinhole structures and macroparticles that may originate from splashing of the target material during the deposition process. Defects due to pinholes and macroparticles are a common characteristic of PVD coatings and are difficult to avoid, but can be minimized by setting optimal deposition parameters [51]. Apart from that, the images inserted in Figure 2(b and d) also show the morphology of TiCN particles which are almost round in shape with a diameter of 0.5-1.0 µm, indicating that film growth occurs through initial nucleation followed by isotropic grain growth [59], [60]. Overall, the success of the TiCN coating on both types of SS substrates is evident from the even distribution of coating particles across the substrate surface. However, the presence of defects, such as pinholes, remains a concern because they can serve as entry points for aggressive ions that cause corrosion, especially in extreme environments such as geothermal fluids, as previously explained. Therefore, even though PVD coating has been successful, optimization of process parameters is still needed to reduce surface defects and thereby improve long-term corrosion performance.

3.2 Coating thickness and microhardness characteristics

Table 2 shows the layer thickness as a function of deposition time, indicating that the TiCN layer thickness on both substrates increases with increasing deposition time. At a coating time of 15 minutes, the SS 18-8 substrate exhibited a slightly higher layer thickness than SS 11-0. This behavior is likely attributed to its higher surface roughness, which provides a greater number of nucleation sites and enhances initial coating growth during the early stage of deposition [61]. However, at a coating time of 25 minutes, the layer thickness on both substrates was almost the same, and at 35 minutes, both showed the same thickness, around 1.65 µm. The coating results show small differences at the initial stage, but as time progresses, the film growth on both substrates tends to balance out.

Table 2. Thickness value of coating characteristic on substrate surface based on various coating deposition times

Sample	Coating Deposition Time (minutes)	Thickness (µm)
SS 11-0	15	0.673
(Ferritic)	25	1.192
	35	1.674
SS-18-8	15	0.751
(Austenitic)	25	1.200
	35	1.672

Based on Table 2 and Figure 3, deposition time affects the layer thickness. Generally, the thickness of the coating is correlated with the resulting hardness, microstructure, and morphology characteristics of the coating [62], [63], [64], [65]. To produce a uniform TiCN layer with optimal performance, have precise control of several deposition parameters (such as duration, temperature, and thermal processing). Based on previous research, longer deposition times have been shown to improve coating uniformity and mechanical properties, whereas insufficient coating duration can lead to uneven thickness, reduced hardness, and the formation of microstructural defects [66]. In this study (see Table 2), both substrates have relatively similar thickness values at each deposition duration. Slight differences in thickness values tend to arise from variations in the steel surface's initial condition, for example, different levels of roughness. These factors, in turn, impact how well the atoms can stick during the coating process. Based on previous research, the presence of complex texture or surface morphology significantly influences both the adhesion process and the layer's bond resistance to the substrate. The uneven surface of the substrate enhances coating adhesion and prolongs coating longevity through physical "locking".

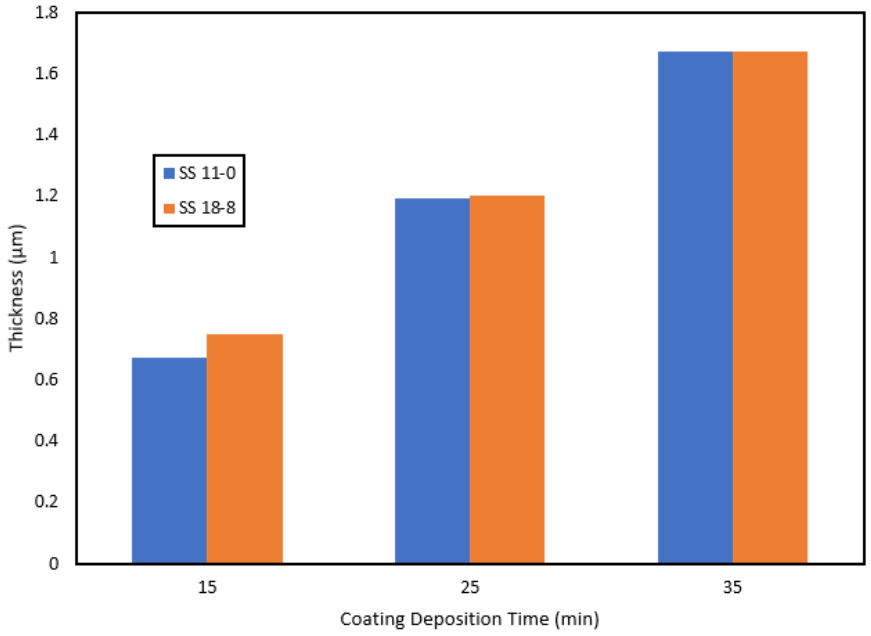

Figure 3. The thickness of the TiCN coating on SS 11-0 and SS 18-8 substrates increases with coating time

Long-term adhesion performance is significantly supported by the physical interconnection (mechanical interlocking) between the coating and the surface of the base material [67]. Previous research indicates a strong relationship between steel surface condition and adhesive bond strength. Through investigation of varying degrees of roughness resulting from mechanical abrasion, Ghumatkar et al. (2017) [68] found the optimal point of adhesion. Using profilometry and tensile

testing, they determined that an average roughness of 1.97 µm was optimal, increasing adhesion through a more effective mechanical attachment mechanism. Similarly, Zielecki et al. (2013) [69] investigated the combined effect of surface roughness and topography on the mechanical strength of steel-to-steel adhesive joints, whose findings highlighted that surface texture and microstructural features, in addition to chemical properties, are critical in strengthening the initial bond and long-term durability of the coating or adhesive. The increase in coating thickness with increasing deposition time confirms that exposure time is a key parameter in the TiCN coating growth process. However, the results also indicate that deposition efficiency is not entirely determined by process parameters but is also influenced by the initial conditions of the substrate. In this context, it is important to consider that surface roughness characteristics can have different effects on coating formation and quality, as previously described.

Table 3 presents the results of Vickers hardness measurements for SS 11-0 and SS 18-8 substrates, in conditions before and after coating process at different coating deposition time variations. The data in Table 3 shows how the coating process (specifically coating deposition time) influences the increase in surface hardness on each type of stainless-steel substrates. Based on Table 3, the SS 11-0 substrate without any coating exhibited an initial hardness of 216.7 HV. After 15 minutes of coating, the hardness increased to 409.9 HV and continued to rise significantly, reaching 1539.6 HV at 25 minutes. However, extending the coating time to 35 minutes did not lead to any further increase, with the hardness remaining at 1539.6 HV. This suggests that the coating system reached saturation in accommodating the TiCN layer, thus further prolonging the deposition time no longer significantly affects hardness. A similar trend was observed for the SS 18-8 substrate, where hardness increased in accordance with the applied surface treatment. These findings are consistent with previous studies, which reported that the longer the deposition time, the more TiCN material accumulates on the substrate surface, resulting in a thicker coating, a denser microstructure, and higher hardness [70], [71]. This happens because more TiCN atoms reach and adhere to the surface over time. These atoms stack and fill surface gaps, creating mechanical interlocking between the coating and the substrate, which strengthens the layer [70], [71]. However, once the substrate reaches a saturation point at which it can no longer accommodate additional TiCN, the growth slows down, and further increasing the deposition time does not significantly improve hardness. This phenomenon has been observed in stainless steel and other metals, highlighting the importance of balancing deposition time with the substrate's capacity to absorb the coating in order to achieve optimal performance.

Table 3. Substrate hardness values before and after coating at various coating deposition time

Coating Deposition Time (minutes)	Microhardness (HV)	
	SS 11-0	SS 18-8
0 (uncoated)	216.7	-
15	409.9	587.5
25	1539.6	2604.7
35	1539.6	3964.1

After measuring the thickness and hardness of TiCN coatings on substrates, substrates with longer coating deposition times exhibited the most optimal combination of characteristics. Although this study did not comprehensively discuss the specific effects of coating time, the results clearly indicate that increasing coating time contributes to an increase in coating thickness and surface hardness [72], [73]. This confirms that coating deposition time is a crucial parameter that directly affects coating functionality, requiring careful consideration in the optimization of TiCN coatings. Based on the literature, increasing coating thickness and hardness is known to be significant in improving the corrosion resistance of metal substrates [74], [75]. More optimal coating thickness serves as a more effective physical barrier against the penetration of corrosive substances such as chloride ions

(Cl^-), water vapor, and oxygen [76], [77]. A sufficiently optimal coating can slow the rate of diffusion of corrosive substances towards the substrate surface, thereby reducing the rate of corrosion reactions that occur at the metal interface. Furthermore, an optimal thickness also helps mask the substrate topography, thereby minimizing the formation of weak points that can become corrosion entry routes. On the other hand, increasing surface hardness provides additional protection against mechanical damage such as abrasion, scratches, and microdeformation, which are usually precursors to the formation of defects or microcracks in protective coatings [78]. Mechanical damage often accelerates the penetration of corrosive media into the substrate. Coatings with high hardness are more resistant to external pressure and friction and are less likely to form microcracks, resulting in better overall resistance to corrosive attack.

Thus, the combination of adequate coating thickness and high surface hardness plays a key role in improving coating integrity, extending component service life, and providing more reliable protection against exposure to aggressive environments, such as in geothermal, marine, and oil and gas industry applications. To represent the optimal performance of the coating system, samples with the most ideal combination of thickness and hardness were selected for further analysis regarding their corrosion performance. The analysis included surface morphology characterization using FESEM after corrosion testing and corrosion resistance evaluation using the salt spray method.

3.3 Elemental mapping and surface morphology for corroded substrate after neutral environment exposure

The effectiveness of the TiCN coating in increasing corrosion resistance was evaluated by comparing the corrosion behavior of stainless-steel substrates 18-8 and 11-0, both before and after coating with TiCN. Figure 4(a–b) sequentially presents the results of elemental mapping on the surfaces of TiCN-coated SS 11-0 and SS 18-8 substrates, and after undergoing corrosion resistance testing, to observe the distribution of elements after exposure to a salt-based corrosive environment (neutral salt spray). Figure 4(a) shows that oxygen is the most dominant element with a percentage of 66.95%, followed by titanium at 21.97%. Meanwhile, the elements carbon and chloride contributed 7.05% and 2.13%, respectively. This composition shows a significant difference compared to the elemental analysis before corrosion performance testing (as shown in Figure 1(c)). High oxygen levels and the presence of chloride ions (Figure 4(a)) indicate significant corrosion. However, because the main elements of the substrate (such as iron or chromium) have not been detected in significant amounts, the TiCN layer still provides partial protection and blocks the entry of aggressive ions. Figure 4(b) indicates that the TiCN-coated SS 18-8 substrate surface has a much better corrosion resistance response than SS 11-0 (see Figure 4(a)). The element mapping results (see Figure 4(b)) show that the coating element (Ti) remains dominant after the corrosion test. This composition is not much different from the EDS results on SS 18-8, which had been coated with TiCN before exposure to a corrosive environment (see Figure 1(d)). Figure 4(b) demonstrates that the TiCN protective layer is stable and resistant to significant degradation due to exposure to saline environments.

Furthermore, the corrosion performance test results, presented in Figure 5(a–d), compare SS substrates without coating with SS substrates coated with TiCN. These data validate previous findings (Figure 4(a-b)) that TiCN coatings effectively protect surfaces from corrosive environmental degradation. Figure 5(a) shows that the uncoated SS 11-0 substrate suffered severe corrosion damage after exposure to a corrosive environment. This is evident in the formation of a thick, dense corrosion layer covering the entire metal surface. Corrosion products appear as rough, spherical lumps tens of micrometers in diameter, which combine to form irregular layers. This shows that corrosion occurs extensively and progressively, and that the metal oxidation process dominates the entire surface. The corrosion products formed are most likely iron and chloride oxides, such as Fe_2O_3, FeOOH, and $FeCl_3$, which are the result of the reaction between Fe from

the substrate and Cl^- ions from NaCl during exposure to a neutral environment [78], [79]. In addition, no intact substrate surface is visible, indicating that Cl^- ions have penetrated the entire surface, accelerated redox reactions, and caused general and local corrosion (pitting). This is consistent with other reports in the literature, which emphasize that chloride ions play a critical role in breaking down passive films on stainless steels, leading to severe pitting and crevice corrosion in saline conditions [79]. Thus, these findings confirm that without protective coatings, 11-0 stainless steel (ferritic) is not suitable for use in high-salinity environments.

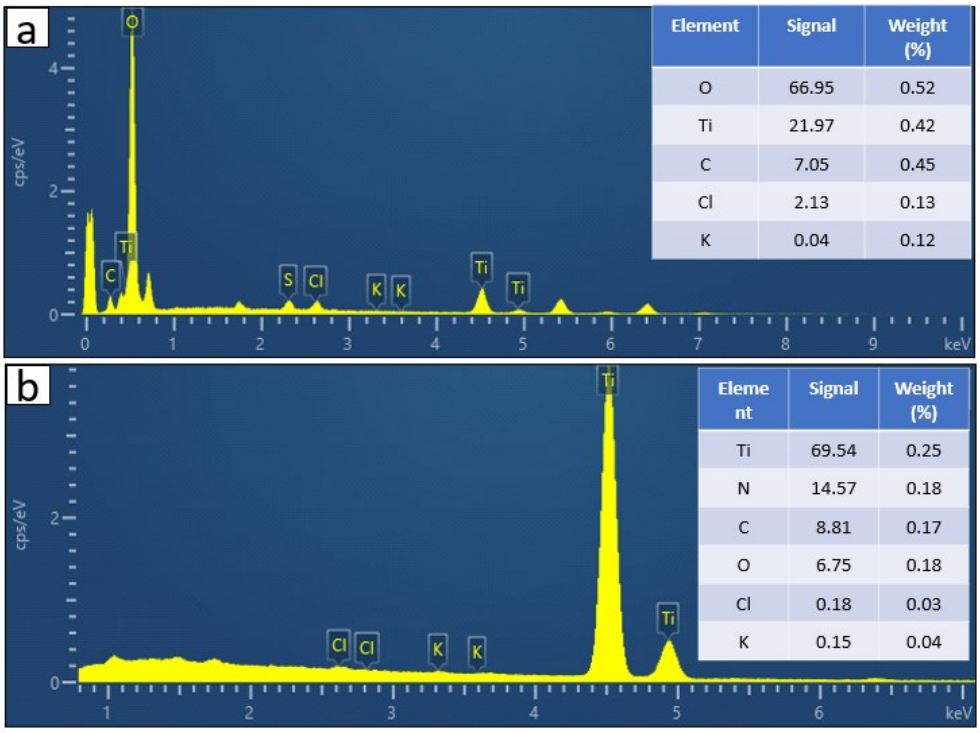

Figure 4. Results of elemental mapping analysis of the surface of SS 11-0 (a) and SS 18-8 (b) after coated with TiCN and after undergoing corrosion resistance testing

In contrast to Figure 5(a), Figure 5(b) shows the surface of SS 11-0, which has been coated with TiCN, and, after exposure to a corrosive environment, exhibits a more controlled level of damage. Although there are visible corrosion products in the form of small granular particles scattered on the surface, these products do not form a massive corrosion layer as seen on uncoated substrates. The uneven distribution of these products indicates localized corrosion. In addition, some parts of the coating layer were observed to peel off, suggesting that, despite its ability to slow corrosion, the coating's adhesion to the substrate still has limitations. According to previous studies, this localized corrosion phenomenon is usually caused by pitting corrosion and coating defects or coating disbondment [44] as shown in Figure 2(b)). Nevertheless, the TiCN coating markedly enhances the corrosion resistance of SS 11-0, making it more reliable in aggressive environments than its uncoated counterpart.

Figure 5(c) illustrates the surface condition of uncoated 18-8 stainless steel after exposure to a corrosive environment. Compared with uncoated 11-0 stainless steel (Figure 5(a)), the corrosion pattern on this specimen is more moderate. Longitudinal traces ("stretch marks") are still visible, indicating that the corrosion products have not completely covered the entire metal substrate. Corrosion seems to only occur in certain spots (locally). Darker areas indicate where corrosion deposits have accumulated. This demonstrates that 18-8 stainless steel still protects itself naturally, even in harsh environments. Its chromium and nickel content help create a strong protective layer of chromium oxide (Cr_2O_3) on the surface, preventing harmful ions such as Cl^- from damaging it.

Although SS 18-8 exhibits better durability, the absence of an additional protective layer allows chloride ions (Cl^-) to penetrate through damage or scratches in the passive layer, which can ultimately lead to long-term pitting corrosion. Therefore, additional coating applications are highly recommended to optimize durability. Figure 5(d) shows the surface of 18-8 stainless steel that has been coated and then exposed to a corrosive environment. The observation results show that the amount of corrosion products formed is lower, and the distribution appears more regular and less dense than that seen in SS 11-0 (compare with Figure 5(a and b)). The corrosion rate of this material is lower than that of SS 11-0 (whether coated with TiCN or not). However, the corrosion process still occurs because the TiCN layer forms an effective barrier against the penetration of Cl^- ions. Meanwhile, the 18-8 substrate still provides backup protection if the coating layer is scratched or partially damaged. This advantage is due to the 18-8 composition, which is rich in chromium and nickel, which helps form a natural passive layer that resists the penetration of corrosive ions [12], [13]. This combination shows very optimal protective performance, making this material very suitable for use in corrosive industrial environments.

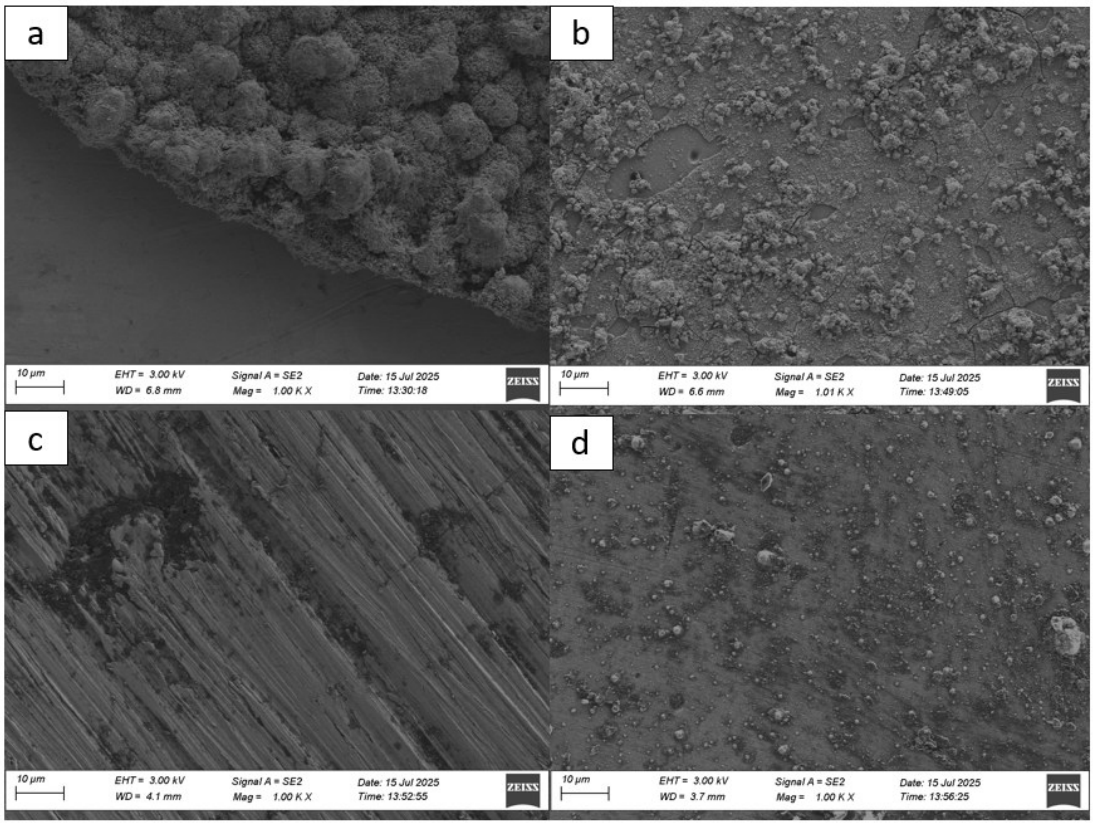

Figure 5. Image of stainless-steel surface after exposure to a corrosive environment: (a) surface morphology of SS 11-0 without coating, (b) surface morphology of coated SS 11-0, (c) surface morphology of SS 18-8 without coating, and (d) surface morphology of coated SS 18-8

Although the corrosion evaluation in this study primarily emphasizes the role of the TiCN coating as the outer protective barrier, the contribution of the substrate composition remains significant, particularly under non-ideal conditions where coating defects such as pinholes, microcracks, or structural discontinuities are present. These defects can act as preferential pathways for the ingress of aggressive species, including chloride ions, thereby enabling localized interaction between the corrosive environment and the underlying substrate. Consequently, the overall corrosion behavior should be interpreted as a coupled response of the coating–substrate system rather than solely the coating. In this context, the corrosion resistance of stainless steel is fundamentally governed by the formation and stability of its passive film in corrosive environments, which typically exhibits a

duplex structure with distinct compositional and functional characteristics [12], [80]. In austenitic stainless steels such as SS 18-8, the passive film generally consists of an outer layer and an inner layer with differing properties [80]. The outer layer is relatively less dense and more reactive due to its direct interaction with the surrounding environment. It is primarily composed of Fe- and Cr-based oxy-hydroxides formed through reactions with water and oxygen. Species such as FeOOH and CrOOH incorporate both oxygen and hydroxyl groups. At the same time, hydroxides such as Fe $(OH)_3$ and Cr $(OH)_3$ form under aqueous conditions and contribute to the initial protective response. However, this outer region is inherently porous and therefore more vulnerable to degradation, particularly in aggressive environments with high chloride ion concentrations. Beneath this outer layer, a more stable and protective inner layer develops, predominantly consisting of chromium oxide (Cr_2O_3) [81]. This inner layer is dense, adherent, and thermodynamically stable, forming directly at the metal–oxide interface. Its compact structure plays a critical role in maintaining passivation by effectively limiting the diffusion of oxygen, water, and aggressive ions toward the substrate, thereby significantly enhancing the corrosion resistance of austenitic stainless steel [81], [82]. In contrast, SS 11-0, a ferritic stainless steel with lower chromium content and no nickel addition, exhibits a reduced ability to form a stable, protective passive film. The passive layer formed on this substrate tends to be thinner, less compact, and more susceptible to breakdown under aggressive conditions, especially in chloride-containing environments. Under defect-assisted exposure, such as in the presence of pinholes or microcracks within the TiCN coating, this limited passivation capability facilitates the initiation of localized corrosion at exposed substrate regions. Moreover, the accumulation of corrosion products beneath the coating may induce volumetric expansion, generating localized mechanical stresses at the coating–substrate interface. These stresses can promote crack initiation, interfacial debonding, and the eventual delamination of the coating. As a result, the TiCN coating deposited on SS 11-0 becomes more susceptible to degradation, leading to a more rapid propagation of localized corrosion compared to the SS 18-8 system [12], [13].

3.4 Corrosion rate performance

The results of the corrosion resistance test (see Table 4) using the salt spray method provide a clear picture of the effects of material type and the influence of TiCN coating on the corrosion rate of SS 11-0 and SS 18-8 substrates. Corrosion resistance is evaluated using the weight-loss method, which quantifies the extent of material degradation due to corrosion. In the SS 18-8 uncoated specimen, a mass loss of 0.0008 grams (0.0028%) was recorded, while the SS 18-8 coated specimen only experienced 0.0006 grams (0.0019%). This difference, although relatively small, shows that coating can reduce the corrosion rate, even on materials that intrinsically have good corrosion resistance, such as SS 18-8. The effectiveness of the coating also appears to be much greater on SS 11-0, where the uncoated specimen shows the highest weight loss, namely 0.0087 grams (0.1960%). In contrast, after being coated, the mass loss decreases drastically to 0.0038 grams (0.0864%).

Table 4. Weight loss data after corrosion performance test

No	Substrate	Mass (g)		Weight Loss (g)	Weight Loss Percentage (%)
		Initial Mass (g)	Final Mass (g)		
1	SS 18-8 Uncoated	28.4088	28.4080	0.0008	0.0028
2	SS 18-8 Coated	31.3475	31.3469	0.0006	0.0019
3	SS 11-0 Uncoated	4.4390	4.4303	0.0087	0.1960
4	SS 11-0 Coated	4.4009	4.3971	0.0038	0.0864

As a continuation of the evaluation of the corrosion test results, the corrosion rate for each substrate was also analyzed, as shown in Figure 6. The corrosion rate data obtained supported the previous weight-loss results (see Table 4), in which the SS 18-8 specimen, both in TiCN-coated and uncoated conditions, showed much lower corrosion rates than uncoated and coated SS 11-0. The uncoated SS 18-8 specimen had a corrosion rate of 0.2600 mm/y, whereas the TiCN coating on SS 18-8 reduced the corrosion rate to 0.1625 mm/y. Based on corrosion resistance standards, the corrosion rate values for both SS 18-8 substrates are categorized as "good", which means that this material can be used in corrosive environments with a relatively long service life. On the other hand, the SS 11-0 specimen showed much lower corrosion resistance. The SS 11-0 substrate without coating has a corrosion rate of 2.8271 mm/y. After being coated, the corrosion rate decreased to 1.1761 mm/y. These results confirm that the surface coating effectively inhibits the rate of corrosion.

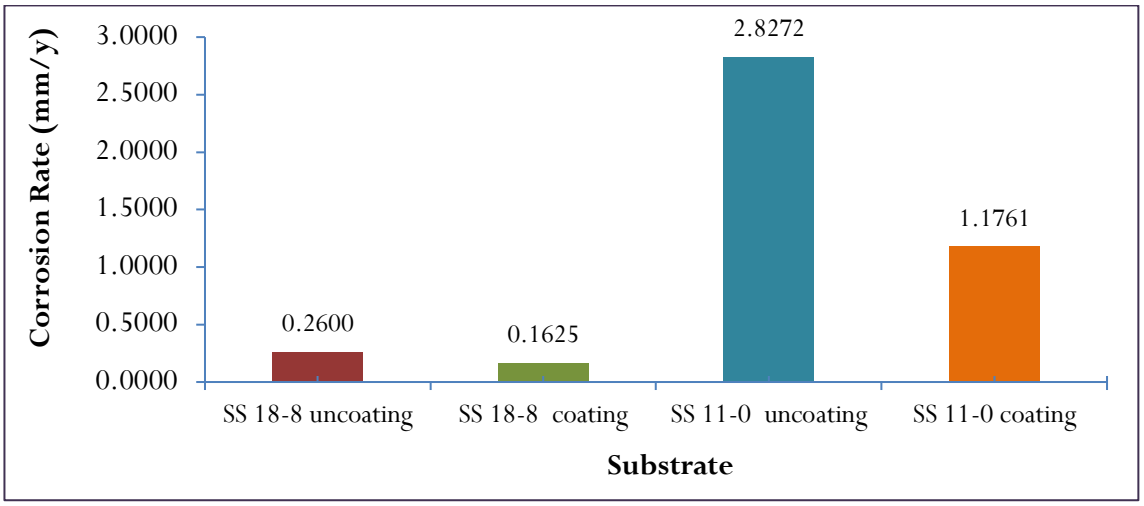

Figure 6. Corrosion rates determined by the weight loss method for coated and uncoated SS 11-0 and SS 18-8 substrates

The trend in corrosion characteristics, as indicated by the polarization resistance method, is consistent with that from the weight-loss method (Table 4). Figure 7(a–d) shows LPR curves of the anodic reaction characteristics during the corrosion process for each substrate. The curve behavior on the uncoated SS 11-0 substrate (Figure 7(a)) shows a smooth current–potential relationship with no plateau region (passivation), indicating that the reaction proceeds stably without the formation of a passive layer [83], [84]. A significant increase in anodic current with increasing potential indicates that the oxidation reaction (metal dissolution) is becoming increasingly dominant. On the coated SS 11-0 substrate (Figure 7(b)), the LPR curve exhibits noticeable fluctuations and deviations from ideal linear behavior, indicating the presence of inhomogeneities or defects in the coating layer, such as pores and microcracks. These irregularities suggest that a stable passive film has not formed effectively and that the coating is not yet fully capable of inhibiting the diffusion of aggressive ions, particularly Cl^-, to the substrate surface [84]. Meanwhile, the uncoated (Figure 7(c)) and coated (Figure 7(d)) SS 18-8 substrates exhibited smaller fluctuations, the presence of passivation, and a more consistent adherence to the general linear trend, with the coated SS 18-8 substrate showing a better linear trend than the uncoated SS 18-8 substrate. Therefore, the coated SS 18-8 substrate exhibits relatively more stable electrochemical behavior than the uncoated SS 18-8 substrate. Although complete passivation has not been clearly demonstrated, these uncoated and coated SS 18-8 substrates show greater stability than SS 11-0, indicating a greater tendency toward passive layer formation.

Furthermore, Table 5 summarizes the relationships among corrosion current density (I_{corr}), polarization resistance (Rp), and corrosion rate (CR in mpy or milli-inches per year), which consistently confirm the previously observed trend in corrosion resistance. Higher current density

(I_{corr}) values reflect a higher rate of electrochemical reaction kinetics, indicating that the metal dissolution occurs more rapidly [21]. Meanwhile, low polarization resistance (Rp) values indicate that charge-transfer resistance at the metal–electrolyte interface is low, facilitating the corrosion reaction [85]. The corrosion current density (I_{corr}) decreased significantly from uncoated SS 11-0 (2,678 nA) to coated SS 18-8 (256.6 nA), indicating that the corrosion reaction rate decreased progressively. This is consistent with the corrosion rate, which also decreased gradually, from 3.059 mpy for uncoated SS 11-0 to just 0.1172 mpy for coated SS 18-8, indicating a significant improvement in corrosion resistance. Conversely, the polarization resistance (Rp) values show an increasing trend, from 9.729 kΩ to 101.5 kΩ, indicating that the material is becoming more resistant to corrosion. The sharp increase in Rp, particularly in the coated SS 18-8, indicates greater resistance to charge transfer on the metal surface, resulting from both the material's intrinsic properties and the presence of a protective coating. The relationship between corrosion current density, polarization resistance, and corrosion rate reinforces and confirms the results of previous analyses, namely that the combination of material composition (higher Cr and Ni content in SS 18-8) and coating protection provides the optimal improvement in corrosion resistance.

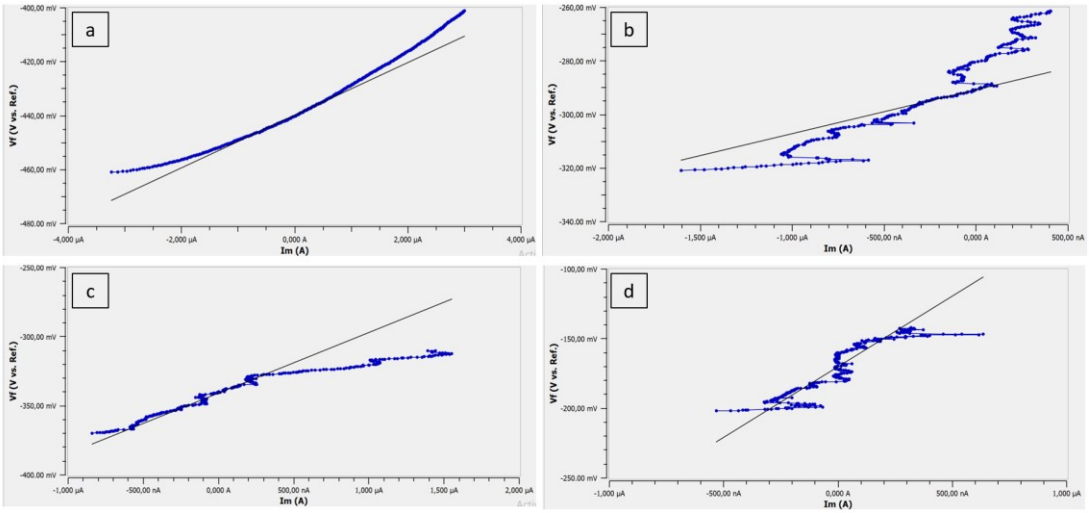

Figure 7. The Linear Polarization Resistance (LPR) curve of the substrates of uncoated SS 11-0 (a), coated SS 11-0 (b), uncoated SS 18-8 (c), and coated SS 18-8 (d)

Table 5. Summary of corrosion current density (I_{corr}), polarization resistance (Rp), and corrosion rate values for coated and uncoated SS 11-0 and SS 18-8 substrates

Variable	Substrates			
	Uncoated SS 11-0	Coated SS 11-0	Uncoated SS 18-8	Coated SS 18-8
I_{corr} (nA)	2678.0	1597.0	595.7	256.6
Corrosion Rate (mpy)	3.0590	0.5499	0.3444	0.1172
Rp (kΩ)	9.729	16.32	43.73	101.5

4. Conclusion

This study successfully demonstrates that TiCN coatings were successfully deposited on SS 11-0 and SS 18-8 substrates using the PVD method. The successful formation of the coating was confirmed by elemental analysis, which identified characteristic TiCN elements, and by morphological observations that revealed differences in surface homogeneity and defect distribution. The coating thickness and hardness increased progressively with longer deposition time, indicating a direct relationship between exposure duration and coating growth. In addition,

the SS 18-8 substrate consistently exhibited higher hardness than SS 11-0 at all deposition intervals, suggesting improved coating quality and interfacial integrity. From a corrosion perspective, the SS 18-8 substrate exhibited superior performance, with corrosion rate values decreasing from 0.2600 mm/y (uncoated) to 0.1625 mm/y after TiCN deposition, both of which were lower than those observed for SS 11-0. This enhanced corrosion resistance is attributed not only to the protective role of the TiCN layer as a diffusion barrier, but also to the intrinsic chemical composition of SS 18-8, which is enriched with chromium and nickel and capable of forming a more stable passive film.

Scientifically, the findings highlight that corrosion resistance in coated systems should be understood as a synergistic response between the coating and the substrate, particularly under non-ideal conditions where defects such as pinholes, pores, or microcracks are present. These defects may act as preferential pathways for aggressive species, thereby exposing the underlying substrate to localized corrosion. In this context, the initial surface condition plays a dual role. A controlled surface roughness can enhance mechanical interlocking and improve coating adhesion during deposition. However, roughness originating from growth-related defects, particularly macroparticles, exhibits fundamentally different characteristics, leading to local inhomogeneity, weak interfacial bonding, and potential initiation sites for coating failure. Under such defect-assisted conditions, the ability of the substrate to maintain a stable passive layer becomes critical. The superior performance of SS 18-8 compared to SS 11-0 confirms that austenitic stainless steel with higher Cr–Ni content is more effective at mitigating localized corrosion even when coating defects are present. From an application standpoint, these results provide important insights for material selection and coating design in aggressive environments, including geothermal, marine, and petrochemical systems. The TiCN/SS 18-8 system demonstrates greater reliability under defect-tolerant conditions, which is highly relevant for long-term service where coating imperfections are often unavoidable. Therefore, optimizing both coating properties and substrate composition is essential to extend service life, reduce maintenance frequency, and improve operational efficiency. These findings are expected to support the development of more robust coating–substrate systems and provide practical guidance for industrial applications requiring enhanced corrosion resistance and durability.

Author's declaration

Author contribution

Agus Solehudin: Conceptualization; Methodology; Supervision; Resources; Validation; and Writing – original draft. **Haipan Salam**: Data curation; Formal analysis; Validation, and Visualization. **Enda Permana**: Data curation; Methodology, Resources; Investigation. **Atiek Rostika Noviyanti**: Supervision; Reviewing and Editing. **Akrajas Ali Umar**: Supervision; Reviewing and Editing. **Risti Ragadhita**: Methodology; Formal analysis; Visualization; and Writing-original draft.

Funding statement

This research was supported by the Institute for Research and Community Service of Universitas Pendidikan Indonesia (grant number: 66/UN04.D/PT.01.01/2025).

Data availability

All data generated or analyzed during this study are included in this published article.

Acknowledgements

The authors would like to thank the Institute for Research and Community Service of Universitas Pendidikan Indonesia, the Corrosion and Coating Laboratory of Universitas Pendidikan Indonesia,

PT Samudra Teknindo Hydraumatic for their assistance in the Physical Vapor Deposition Coating (PVD), and all who have supported this research.

Competing interest

The authors declare no conflicts of interest in this research.

Ethical clearance

Not applicable.

AI statement

Artificial intelligence (AI)-assisted tools were used exclusively to support language editing during the preparation of this manuscript. Grammarly was used to review grammar, spelling, punctuation, and overall language accuracy, while ChatGPT was employed solely to improve the coherence, cohesiveness, and readability of the text. To ensure the linguistic accuracy and clarity, the manuscript was further reviewed by an English language expert. All scientific analyses, interpretations, discussions, and conclusions were developed independently by the authors, who retained full responsibility for the content of the manuscript. This manuscript represents the authors' original work derived from an original study, and no textual content, data, tables, figures, or graphical materials were generated by artificial intelligence.

Publisher's and Journal's note

Universitas Negeri Padang as the publisher, and Editor of Teknomekanik state that there is no conflict of interest towards this article publication.

References

[1] G. Oppong Boakye, E. O. Straume, D. Kovalov, and S. N. Karlsdottir, "Wear-reducing nickel-phosphorus and graphene oxide-based composite coatings: Microstructure and corrosion behavior in high temperature geothermal environment," *Corros. Sci.*, vol. 209, no. October, p. 110809, 2022, https://doi.org/10.1016/j.corsci.2022.110809

[2] H. Sadeghi and R. M. Singh, "Driven precast concrete geothermal energy piles: Current state of knowledge," *Building and Environment*, vol. 228. Elsevier Ltd, Jan. 15, 2023. https://doi.org/10.1016/j.buildenv.2022.109790

[3] F. Al Mubarak, R. Rezaee, and D. A. Wood, "Economic, Societal, and Environmental Impacts of Available Energy Sources: A Review," *Eng*, vol. 5, no. 3, pp. 1232–1265, 2024, https://doi.org/10.3390/eng5030067

[4] W. A. Elders, D. Nielson, P. Schiffman, and A. Schriener, "Investigating ultra high-enthalpy geothermal systems: A collaborative initiative to promote scientific opportunities," *Scientific Drilling*, vol. 18, pp. 35–42, 2014, https://doi.org/10.5194/sd-18-35-2014

[5] J. Thevakumar, J. Owen, K. Purnell, E. Barmatov, and R. Barker, "Assessment of carbon steel and corrosion resistant alloy corrosion in geothermal environments containing sulphuric acid," *Corros. Sci.*, vol. 257, no. September, p. 113319, 2025, https://doi.org/10.1016/j.corsci.2025.113319

[6] H. Bai *et al.*, "Effect of Surface Roughness on Static Corrosion Behavior of J55 Carbon Steel in CO2-Containing Geothermal Water at 65 °C," *Coatings*, vol. 13, no. 5, May 2023, https://doi.org/10.3390/coatings13050821

[7] C. Rica, G. L. Rowe, S. L. Brantley, J. F. Fernandezb, and A. Borgia, "The chemical and hydrologic structure of PO & Volcano," *Journal of Volcanology and Geothermal Research*, vol. 64, ssues 3–4, pp. 233–267, 1995. https://doi.org/10.1016/0377-0273(94)00079-V

[8] I. Maior *et al.*, "Chemical Composition and Corrosion—Contributions to a Sustainable Use of Geothermal Water," *Energies (Basel).*, vol. 18, no. 14, Jul. 2025, https://doi.org/10.3390/en18143634

[9] I. O. Thorbjornsson *et al.*, "Materials investigation of the high temperature IDDP-1 wellhead," *Geothermics*, vol. 87, no. April, p. 101866, 2020, https://doi.org/10.1016/j.geothermics.2020.101866

[10] A. Sasi, R. J. Vikram, and K. Dash, "Corrosion and oxidation behavior of high entropy alloys in extreme and harsh environments: A perspective on steam corrosion," *Journal of Applied Physics*, vol. 138, no. 2. American Institute of Physics, Jul. 14, 2025. https://doi.org/10.1063/5.0273671

[11] F. Brownlie, T. Hodgkiess, A. Pearson, and A. M. Galloway, "A study on the erosion-corrosion behaviour of engineering materials used in the geothermal industry," *Wear*, vol. 477, no. March, p. 203821, 2021, https://doi.org/10.1016/j.wear.2021.203821

[12] J. Šćepanović, B. Zindović, D. Radonjić, M. R. Pantović Pavlović, and M. M. Pavlović, "Influence of organic/inorganic inhibitors on AISI 304 (1.4301) and AISI 314 (1.4841) steels corrosion kinetics in nitric acid solution," *Journal of the Serbian Chemical Society*, vol. 89, no. 9, pp. 1191–1210, 2024, https://doi.org/10.2298/JSC240514076S

[13] X. man ZHANG, Z. yu CHEN, H. feng LUO, T. ZHOU, Y. liang ZHAO, and Z. cheng LING, "Corrosion resistances of metallic materials in environments containing chloride ions: A review," *Transactions of Nonferrous Metals Society of China (English Edition)*, vol. 32, no. 2, pp. 377–410, Feb. 2022, https://doi.org/10.1016/S1003-6326(22)65802-3

[14] E. Ahmed, J. Liu, and J. Liu, "Mitigating Corrosion in Downhole Environments of Oil and Gas Operations: Mechanisms, Challenges, and Control Strategies," *Trends in Sciences*, vol. 22, no. 8, 2025, https://doi.org/10.48048/tis.2025.9855

[15] R. Bender *et al.*, "Corrosion challenges towards a sustainable society," *Materials and Corrosion*, vol. 73, no. 11, pp. 1730–1751, 2022, https://doi.org/10.1002/maco.202213140

[16] F. Ge *et al.*, "Microstructure and Properties of TiN/TiCN/Al2O3/TiN Coating Enhanced by High-Current Pulsed Electron Beam," *Coatings*, vol. 14, no. 4, Apr. 2024, https://doi.org/10.3390/coatings14040378

[17] P. Yang, N. Q. Nguyen, Z. A. Wong, Y. Morimoto, and I. V Zenyuk, "Electrochemical Analysis and Surface Steel for Proton Exchange Membrane Fuel Cell Electrochemical Analysis and Surface Characterization of TiCN", https://doi.org/10.1149/1945-7111/ae492c

[18] J. Lou, Z. Gao, J. Zhang, H. He, and X. Wang, "Comparative investigation on corrosion resistance of stainless steels coated with titanium nitride, nitrogen titanium carbide and titanium-diamond-like carbon films," *Coatings*, vol. 11, no. 12, 2021, https://doi.org/10.3390/coatings11121543

[19] T. Miller, J. M. Lin, L. Pirolli, L. Coquilleau, R. Luharuka, and A. V. Teplyakov, "Investigation of thin titanium carbonitride coatings deposited onto stainless steel," in *Thin Solid Films*, Nov. 2012, pp. 193–198. https://doi.org/10.1016/j.tsf.2012.08.012

[20] G. Kumaresan, E. M. Jawahar, and P. Senthilkumar, "TiN and TiCN Coated Stainless Steel 316 Ultrosonic Cavitation Probe for High Temperature Application," *Silicon*, vol. 11, no. 2, pp. 713–719, Apr. 2019, https://doi.org/10.1007/s12633-018-9952-7

[21] D. Rahmadiawan, S. C. Shi, and W. T. Zhuang, "Reinforcing polyvinyl alcohol films with layered double hydroxide and tannic acid to enhance tensile strength, tribological performance, and corrosion resistance in biomedical coating applications," *Mater. Res. Express*, vol. 11, no. 11, 2024, https://doi.org/10.1088/2053-1591/ad8f94

[22] M. Okayasu and D. Ishida, "Effect of Microstructural Characteristics on Mechanical Properties of Austenitic, Ferritic, and γ-α Duplex Stainless Steels," *Metall. Mater. Trans. A Phys. Metall. Mater. Sci.*, vol. 50, no. 3, pp. 1380–1388, 2019, https://doi.org/10.1007/s11661-018-5083-4

[23] Y. Shimomura, H. W. Park, and J. Yanagimoto, "Hot deformation behavior of ferrite and austenite phases of ferritic stainless steel in the duplex temperature range," *Materials Science and Engineering: A*, vol. 923, no. December 2024, p. 147698, 2025, https://doi.org/10.1016/j.msea.2024.147698

[24] R. Mariappan, S. Kumaran, and T. S. Rao, "Effect of sintering atmosphere on structure and properties of austeno-ferritic stainless steels," *Materials Science and Engineering: A*, vol. 517, no. 1–2, pp. 328–333, 2009, https://doi.org/10.1016/j.msea.2009.04.011

[25] J. Che, P. Yi, L. Peng, and X. Lai, "Impact of pressure on carbon films by PECVD toward high deposition rates and high stability as metallic bipolar plate for PEMFCs," *Int. J. Hydrogen Energy*, vol. 45, no. 32, pp. 16277–16286, 2020, https://doi.org/10.1016/j.ijhydene.2020.04.078

[26] Q. Xiao, H. He, S. Shao, J. Shao, and Z. Fan, "Influences of deposition rate and oxygen partial pressure on residual stress and microstructure of YSZ thin films," *Thin Solid Films*, vol. 517, no. 15, pp. 4295–4298, 2009, https://doi.org/10.1016/j.tsf.2008.11.138

[27] N. Li, J. P. Allain, and D. N. Ruzic, "Enhancement of aluminum oxide physical vapor deposition with a secondary plasma," *Surf. Coat. Technol.*, vol. 149, no. 2–3, pp. 161–170, 2002, https://doi.org/10.1016/S0257-8972(01)01446-3

[28] K. Aouadi, B. Tlili, C. Nouveau, A. Besnard, M. Chafra, and R. Souli, "Influence of Substrate Bias Voltage on Corrosion and Wear Behavior of Physical Vapor Deposition CrN Coatings," *J. Mater. Eng. Perform.*, vol. 28, no. 5, pp. 2881–2891, 2019, https://doi.org/10.1007/s11665-019-04033-y

[29] M. Vorobyova *et al.*, "PVD for Decorative Applications: A Review," *Materials*, vol. 16, no. 14, 2023, https://doi.org/10.3390/ma16144919

[30] N. Mahne, M. Čekada, and M. Panjan, "Total and Differential Sputtering Yields Explored by SRIM Simulations," *Coatings*, vol. 12, no. 10, pp. 1–32, 2022, https://doi.org/10.3390/coatings12101541

[31] S. Mirzaei *et al.*, "Effect of substrate bias voltage on the composition, microstructure and mechanical properties of W-B-C coatings," *Appl. Surf. Sci.*, vol. 528, p. 146966, 2020, https://doi.org/10.1016/j.apsusc.2020.146966

[32] M. J. Carmezim, A. M. Simões, M. F. Montemor, and M. Da Cunha Belo, "Capacitance behaviour of passive films on ferritic and austenitic stainless steel," *Corros. Sci.*, vol. 47, no. 3 SPEC. ISS., pp. 581–591, 2005, https://doi.org/10.1016/j.corsci.2004.07.002

[33] C. R. F. Azevedo and A. F. Padilha, "The most frequent failure causes in super ferritic stainless steels: Are they really super?," *Procedia Structural Integrity*, vol. 17, pp. 331–338, 2019, https://doi.org/10.1016/j.prostr.2019.08.044

[34] K. A. Cashell and N. R. Baddoo, "Ferritic stainless steels in structural applications," *Thin-Walled Structures*, vol. 83, pp. 169–181, 2014, https://doi.org/10.1016/j.tws.2014.03.014

[35] A. Di Schino, M. G. Mecozzi, M. Barteri, and J. M. Kenny, "Solidification mode and residual ferrite in low-Ni austenitic stainless steels," *J. Mater. Sci.*, vol. 35, no. 2, pp. 375–380, 2000, https://doi.org/10.1023/A:1004774130483

[36] R. Darolia, "Development of strong, oxidation and corrosion resistant nickel-based superalloys: critical review of challenges, progress and prospects," *International Materials Reviews*, vol. 64, no. 6, pp. 355–380, 2019, https://doi.org/10.1080/09506608.2018.1516713

[37] D. Wang, Q. Zhong, J. Yang, and S. Zhang, "Effects of Cr and Ni on the microstructure and corrosion resistance of high-strength low alloy steel," *Journal of Materials Research and Technology*, vol. 23, pp. 36–52, 2023, https://doi.org/10.1016/j.jmrt.2022.12.191

[38] L. H. Campos Becerra, *A review of heat treatments applied to low and medium and high carbon steels used in cold drawn*, vol. 5, no. 1. Springer International Publishing, 2025. https://doi.org/10.1007/s43939-025-00261-3

[39] H. Tian, J. Wang, Z. Liu, and P. Han, "Effect of Nitrogen on the Corrosion Resistance of 6Mo Super Austenitic Stainless Steel," *Metals (Basel).*, vol. 14, no. 4, 2024, https://doi.org/10.3390/met14040391

[40] J. Ren *et al.*, "Effect of Boron Addition on the Oxide Scales Formed on 254SMO Super Austenitic Stainless Steels in High-Temperature Air," *Metals (Basel).*, vol. 13, no. 2, 2023, https://doi.org/10.3390/met13020258

[41] C. Zhu *et al.*, "Control of the concentrated-precipitation behaviour of Cr23C6 and its effect on the microstructure and properties of S600E sorbitic stainless steel," *Journal of Materials Research and Technology*, vol. 33, no. August, pp. 7193–7205, 2024, https://doi.org/10.1016/j.jmrt.2024.11.085

[42] M. Sumita, T. Hanawa, and S. H. Teoh, "Development of nitrogen-containing nickel-free austenitic stainless steels for metallic biomaterials - Review," *Materials Science and Engineering C*, vol. 24, no. 6-8 SPEC. ISS., pp. 753–760, 2004, https://doi.org/10.1016/j.msec.2004.08.030

[43] S. Kiremit *et al.*, "Development of an In Situ Micro-Corrosion Cell for the Investigation of Pitting Corrosion on Austenitic and Ferritic Stainless Steels," *Corrosion and Materials Degradation*, vol.4, no.1 pp. 104–119, 2023. https://doi.org/10.3390/cmd4010007

[44] A. Royani, S. Prifiharni, and G. Priyotomo, "Corrosion Behavior of Low Carbon Steel Pipe in Condensate Environment," *Trends Sci.* vol. 19, no. 3, pp. 1–11, 2022. https://doi.org/10.48048/tis.2022.2072

[45] G. M. Uddin *et al.*, "Experimental investigation of tribo-mechanical and chemical properties of TiN PVD coating on titanium substrate for biomedical implants manufacturing," *International Journal of Advanced Manufacturing Technology*, vol. 102, no. 5–8, pp. 1391–1404, 2019, https://doi.org/10.1007/s00170-018-03244-2

[46] G. Godwin and M. Shunmuga Priyan, "On PVD coating technique for tribological, bio-compatibility, and corrosion behavior of Ti-based alloys using biomedical applications: A review," *Journal of Materials and Manufacturing*, vol. 3, no. 2, pp. 41–58, 2024, https://doi.org/10.5281/zenodo.14274805

[47] P. Panjan, A. Drnovšek, N. Mahne, M. Čekada, and M. Panjan, "Surface topography of pvd hard coatings," *Coatings*, vol. 11, no. 11, 2021, https://doi.org/10.3390/coatings11111387

[48] O. Knudsen, C. H. M. Hagen, A. W. B. Skilbred, T. K. Bruaas, and J. Nærland, "Root causes for corrosion on painted steel structures in marine environments," *Materials and Corrosion*, vol. 76, no. 6, pp. 802–811, 2025, https://doi.org/10.1002/maco.202314046

[49] B. Tzaneva *et al.*, "Corrosion Properties and Performance of Nanostructured Multilayered Chromium–Amorphous Carbon Coatings on HS6-5-2 Steel," *Metals (Basel).*, vol. 16, no. 2, pp. 1–17, 2026, https://doi.org/10.3390/met16020149

[50] O. Kaya *et al.*, "2D hexagonal boron nitride-based anticorrosion coatings," *JPhys Materials*, vol. 8, no. 4, pp. 0–28, 2025, https://doi.org/10.1088/2515-7639/ae0f53

[51] Z. Dadashi Shanbaraki, M. Azadi, and A. Hafazeh, "Electrochemical characteristics of nano-structure TiCN coatings on the tool steel deposited by PACVD in various solutions," *Results Chem.*, vol. 7, no. March, p. 101531, 2024, https://doi.org/10.1016/j.rechem.2024.101531

[52] P. Panjan, A. Drnovšek, P. Gselman, M. Čekada, and M. Panjan, *Review of growth defects in thin films prepared by PVD techniques*, vol. 10, no. 5. 2020. https://doi.org/10.3390/COATINGS10050447

[53] S. H. Ahn, J. H. Lee, J. G. Kim, and J. G. Han, "Localized corrosion mechanisms of the multilayered coatings related to growth defects," *Surf. Coat. Technol.*, vol. 177–178, pp. 638–644, 2004, https://doi.org/10.1016/S0257-8972(03)00939-3

[54] M. Zou, S. Beckford, R. Wei, C. Ellis, G. Hatton, and M. A. Miller, "Effects of surface roughness and energy on ice adhesion strength," *Appl. Surf. Sci.*, vol. 257, no. 8, pp. 3786–3792, 2011, https://doi.org/10.1016/j.apsusc.2010.11.149

[55] A. Baldelli, J. Ou, D. Barona, W. Li, and A. Amirfazli, "Sprayable, Superhydrophobic, Electrically, and Thermally Conductive Coating," *Adv. Mater. Interfaces*, vol. 8, no. 2, pp. 1–9, 2021, https://doi.org/10.1002/admi.201902110

[56] N. P. Padture, M. Gell, and E. H. Jordan, "Thermal barrier coatings for gas-turbine engine applications," *Science (1979).*, vol. 296, no. 5566, pp. 280–284, 2002, https://doi.org/10.1126/science.1068609

[57] Y. Luo *et al.*, "Superior interface adhesion and protective mechanism of room-temperature-curable polymer composite coating on engineering substrates with lower roughness," *Polym. Test.*, vol. 134, no. January, p. 108430, 2024, https://doi.org/10.1016/j.polymertesting.2024.108430

[58] J. Fu, H. Yu, L. Wang, R. Liang, C. Zhang, and M. Jin, "Preparation and properties of UV-curable polyurethane acrylate / SiO2 composite hard coatings," *Prog. Org. Coat.*, vol. 153, no. February, p. 106121, 2021, https://doi.org/10.1016/j.porgcoat.2020.106121

[59] Y. Qin, J. He, F. Yin, F. Zhang, and B. Liu, "Influence of initial Ti particle size on microstructure and fracture toughness of reactive plasma sprayed TiCN coatings," *Surf. Coat. Technol.*, vol. 325, pp. 482–489, 2017, https://doi.org/10.1016/j.surfcoat.2017.07.001

[60] X. L. Li, C. X. Wang, and G. W. Yang, "Thermodynamic theory of growth of nanostructures," *Prog. Mater. Sci.*, vol. 64, pp. 121–199, 2014, https://doi.org/10.1016/j.pmatsci.2014.03.002

[61] V. Gareyan and Z. Gevorkian, "Impact of surface roughness on light absorption," *Phys. Rev. A (Coll. Park).*, vol. 109, no. 1, 2024, https://doi.org/10.1103/PhysRevA.109.013515

[62] G. Sundararajan and L. Rama Krishna, "Mechanisms underlying the formation of thick alumina coatings through the MAO coating technology," *Surf. Coat. Technol.*, vol. 167, no. 2–3, pp. 269–277, 2003, https://doi.org/10.1016/S0257-8972(02)00918-0

[63] H. Ashassi-Sorkhabi and S. H. Rafizadeh, "Effect of coating time and heat treatment on structures and corrosion characteristics of electroless Ni-P alloy deposits," *Surf. Coat. Technol.*, vol. 176, no. 3, pp. 318–326, 2004, https://doi.org/10.1016/S0257-8972(03)00746-1

[64] W. Liao *et al.*, "Nanocrystalline high-entropy alloy (CoCrFeNiAl0.3) thin-film coating by magnetron sputtering," *Thin Solid Films*, vol. 638, pp. 383–388, 2017, https://doi.org/10.1016/j.tsf.2017.08.006

[65] C. Wang *et al.*, *The resistivity–temperature behavior of AlxCoCrFeNi high-entropy alloy films*, vol. 700. Elsevier B.V., 2020. https://doi.org/10.1016/j.tsf.2020.137895

[66] C. duo Dai, Y. Fu, J. xiang Guo, and C. wei Du, "Effects of substrate temperature and deposition time on the morphology and corrosion resistance of FeCoCrNiMo0.3 high-entropy alloy coating fabricated by magnetron sputtering," *International Journal of Minerals, Metallurgy and Materials*, vol. 27, no. 10, pp. 1388–1397, 2020, https://doi.org/10.1007/s12613-020-2149-2

[67] J. P. B. van Dam, S. T. Abrahami, A. Yilmaz, Y. Gonzalez-Garcia, H. Terryn, and J. M. C. Mol, "Effect of surface roughness and chemistry on the adhesion and durability of a steel-epoxy adhesive interface," *Int. J. Adhes. Adhes.*, vol. 96, p. 102450, 2020, https://doi.org/10.1016/j.ijadhadh.2019.102450

[68] A. Ghumatkar, R. Sekhar, and S. Budhe, "Experimental study on different adherend surface roughness on the adhesive bond strength," *Mater. Today Proc.*, vol. 4, no. 8, pp. 7801–7809, 2017, https://doi.org/10.1016/j.matpr.2017.07.115

[69] W. Zielecki, P. Pawlus, R. PerŁowski, and A. Dzierwa, "Surface topography effect on strength of lap adhesive joints after mechanical pre-treatment," *Archives of Civil and Mechanical Engineering*, vol. 13, no. 2, pp. 175–185, 2013, https://doi.org/10.1016/j.acme.2013.02.005

[70] M. A. Butt, "Thin-Film Coating Methods: A Successful Marriage of High-Quality and Cost-Effectiveness—A Brief Exploration," *Coatings*, vol. 12, no. 8, 2022, https://doi.org/10.3390/coatings12081115

[71] J. C. Avelar-Batista *et al.*, "Effect of coating thickness and deposition methods on the stripping rate of Cr-N coatings," *Surf. Coat. Technol.*, vol. 200, no. 5–6, pp. 1842–1848, 2005, https://doi.org/10.1016/j.surfcoat.2005.08.009

[72] M. Amer, Q. Hayat, V. Janik, N. Jennett, J. Nottingham, and M. Bai, "A Review on In Situ Mechanical Testing of Coatings," *Coatings*, vol. 12, no. 3, pp. 1–34, 2022, https://doi.org/10.3390/coatings12030299

[73] K. K. Maniam and S. Paul, "Corrosion Performance of Electrodeposited Zinc and Zinc-Alloy Coatings in Marine Environment," pp. 163–189, 2021.

[74] W. Handoko, F. Pahlevani, and V. Sahajwalla, "Enhancing corrosion resistance and hardness properties of carbon steel through modification of microstructure," *Materials*, vol. 11, no. 12, 2018, https://doi.org/10.3390/ma11122404

[75] B. Yin *et al.*, "Influence of layer thickness on formation quality, microstructure, mechanical properties, and corrosion resistance of WE43 magnesium alloy fabricated by laser powder bed fusion," *Journal of Magnesium and Alloys*, vol. 12, no. 4, pp. 1367–1385, 2024, https://doi.org/10.1016/j.jma.2022.09.016

[76] L. Zendejas Medina *et al.*, "Enhancing corrosion resistance, hardness, and crack resistance in magnetron sputtered high entropy CoCrFeMnNi coatings by adding carbon," *Mater. Des.*, vol. 205, 2021, https://doi.org/10.1016/j.matdes.2021.109711

[77] M. V. Tavares da Costa, J. Bolinsson, R. C. Neagu, P. Fayet, and E. K. Gamstedt, "Experimental assessment of micromechanical models for fragmentation analysis of thin metal oxide coatings on polymer films under uniaxial tensile deformation," *Surf. Coat. Technol.*, vol. 370, no. March, pp. 374–383, 2019, https://doi.org/10.1016/j.surfcoat.2019.03.035

[78] R. J. K. Wood, "Tribo-corrosion of coatings: A review," *J. Phys. D Appl. Phys.*, vol. 40, no. 18, pp. 5502–5521, 2007, https://doi.org/10.1088/0022-3727/40/18/S10

[79] I. Hamidah *et al.*, "Corrosion of copper alloys in KOH, NaOH, NaCl, and HCl electrolyte solutions and its impact to the mechanical properties," *Alexandria Engineering Journal*, vol. 60, no. 2, pp. 2235–2243, 2021, https://doi.org/10.1016/j.aej.2020.12.027

[80] R. T. Loto, S. Oladipupo, T. Folarin, and E. Okosun, "Impact of chloride concentrations on the electrochemical performance and corrosion resistance of austenitic and ferritic stainless steels in acidic chloride media," *Discover Applied Sciences*, vol. 7, no. 7, 2025, https://doi.org/10.1007/s42452-025-07234-4

[81] R. H. Jung, H. Tsuchiya, and S. Fujimoto, "Growth process of passive films on austenitic stainless steels under wet-dry cyclic condition," *ISIJ International*, vol. 52, no. 7, pp. 1356–1361, 2012, https://doi.org/10.2355/isijinternational.52.1356

[82] L. Freire *et al.*, "Electrochemical and analytical investigation of passive films formed on stainless steels in alkaline media," *Cem. Concr. Compos.*, vol. 34, no. 9, pp. 1075–1081, 2012, https://doi.org/10.1016/j.cemconcomp.2012.06.002

[83] M. B. L. Carvalho, I. S. Bott, A. B. Forero, and J. A. C. Ponciano, "The Corrosion Process of an API 5L X80 Welded Joint in a System with Different pH and H2S Concentration," *Materials Research*, vol. 25, no. Table 1, pp. 1–11, 2022, https://doi.org/10.1590/1980-5373-MR-2021-0443

[84] C. Wang, P. Kusdiyarto, and Y. Li, "Potentiodynamic polarization analysis with various corrosion inhibitors on A508 / IN-182 / IN-52M / 308L / 316L welds," *Kuwait Journal of Science*, vol. 51, no. 2, p. 100202, 2024, https://doi.org/10.1016/j.kjs.2024.100202

[85] S. Zhao, Y. Jing, X. He, and F. Li, "Effect of electrochemical water treatment processes on carbon steel corrosion in urban water supply system," *npj Mater Degrad*, vol 10, no, 23 pp. 1–10, 2026. https://doi.org/10.1038/s41529-026-00736-5